

Shell effect in $A = 116\text{--}124$ Tin isotopes investigated using isotopic analysis of proton scattering at 295 MeV

Yoshiko Kanada-En'yo

Department of Physics, Kyoto University, Kyoto 606-8502, Japan

Proton elastic scattering off Sn isotopes at $E_p = 295$ MeV in the mass number range of $A = 116\text{--}124$ was investigated using calculation employing relativistic impulse approximation (RIA) with theoretical densities obtained for the Sn isotopes from relativistic Hartree-Bogoliubov (RHB) and nonrelativistic Skyrme Hartree-Fock-Bogoliubov (SHFB) calculations of spherical nuclei. In the RIA calculations, a modified version of the Murdock and Horowitz model that includes a density dependence in the effective nucleon-nucleon (NN) interaction was used. A calculation using the theoretical density obtained from a relativistic calculation employing the DD-ME2 interaction successfully reproduced the experimental data for $^{122}\text{Sn}(p, p)$, but it overestimated the $^{116}\text{Sn}(p, p)$ and $^{118}\text{Sn}(p, p)$ cross sections at backward angles. I found the normalization of the experimental $^{120}\text{Sn}(p, p)$ and $^{124}\text{Sn}(p, p)$ cross sections to be inconsistent with the data for the other Sn isotopes, suggesting that it should be corrected. Isotopic analyses of the (p, p) reactions combined with nuclear structure properties were performed based on reaction calculations that used a model density modified from the DD-ME2 density to optimize the neutron density of the Sn isotopes by fitting the isotopic cross section ratios. The resulting optimized density reproduced the experimental (p, p) data for the series of Sn isotopes from ^{116}Sn to ^{124}Sn . The neutron root-mean-square (rms) radii and the skin thickness of the Sn isotopes obtained in the present analysis exhibited smooth A dependences in the range of $A = 116\text{--}124$, which are consistent with the theoretical predictions obtained using the DD-ME2 interaction but seem to contradict the experimental results determined from the (p, p) data. In a detailed analysis of the surface neutron density probed by proton elastic scattering, a signal of the shell effect at $N = 66$ in Sn isotopes was found.

I. INTRODUCTION

The neutron skin thickness Δr_{np} in $N > Z$ nuclei has recently emerged as an issue in understanding the neutron-matter equation of state involving symmetry energy parameters that are connected with Δr_{np} through predictions of theoretical structure calculations [1–3]. Various experiments have been performed to determine Δr_{np} . For example, experimental values of Δr_{np} in Sn and Pb isotopes have been obtained by measuring proton elastic scattering [4–7], X -rays from antiprotonic atoms [8, 9], parity-violating electron scattering [10], pionic probes [11, 12], spin-dipole resonances measured with the $(^3\text{He}, t)$ charge-exchange reaction [13], and electric dipole polarization measured with polarized-proton inelastic scattering [14, 15].

The proton elastic scattering is a useful tool not only for determining the neutron skin thickness of an atomic nucleus but also for probing the density profile of the nucleus in detail—in particular, the surface neutron density—as has been done for various nuclei. For example, the experimental cross sections and analyzing powers measured with (p, p) reactions at $E_p = 800$ MeV [4, 16, 17], 650 MeV [4, 16, 17], and 295 MeV [5, 7, 18] have been utilized to extract the neutron density via reaction analyses. For the analyses of proton elastic scattering in the energy range of $E_p = 100\text{--}400$ MeV, Murdock and Horowitz proposed a reaction model based on the relativistic impulse approximation (RIA), with a meson-exchange model of effective nucleon-nucleon (NN) interactions (the MH model) [19–21]. The original MH model was tuned by globally fitting the (p, p) data, and the com-

putational code for RIA+MH calculation has been widely used for the analyses of (p, p) reactions. Later, Sakaguchi and his collaborators proposed a modified version of the MH model that includes a density dependence of the effective NN interaction [5, 7, 22]; this is called the ddMH model in this paper. The ddMH model was calibrated with experimental $^{58}\text{Ni}(p, p)$ data at 295 MeV for scattering angles $\theta_{\text{c.m.}} \lesssim 50^\circ$, and it successfully described the 295 MeV (p, p) reactions of various target nuclei, including Sn [5], Pb [7], and Ca [18] isotopes.

In a previous paper [23], I proposed a new method of reaction analysis that combines the proton elastic scattering with the isotopic systematics of nuclear structure for a series of isotopes. The method has been applied to the analysis of $^{204}\text{Pb}(p, p)$, $^{206}\text{Pb}(p, p)$, and $^{208}\text{Pb}(p, p)$ at 295 MeV to obtain improved neutron densities and the root-mean-square (rms) radii of the Pb isotopes from the experimental data. It has proven to be a useful tool for extracting neutron densities and rms radii from (p, p) cross sections for a series of isotopes, with less model dependence. Moreover, it can be applied to (p, p) reactions to determine the neutron skin thickness of other series of isotopes. An advantage of the isotopic analysis is that systematic errors in the experimental data obtained using the same experimental setup can be reduced.

In this work, the 295-MeV proton scattering off Sn isotopes in the range $A = 116\text{--}124$ is investigated, for which high-quality data have been obtained from the experiment by Terashima *et al.* [5]. The structure of the Sn isotopes is calculated by using both relativistic Hartree-Bogoliubov (RHB) and nonrelativistic Skyrme Hartree-Fock-Bogoliubov (SHFB) calculations of spherical nuclei.

Using theoretical densities, the $\text{Sn}(p, p)$ reactions are calculated with the RIA+ddMH model in the same way as done in the previous paper [23]. By comparing the theoretical results with the experimental (p, p) data, the isotopic systematics of the structure and reaction properties are investigated. The isotopic analysis is performed using a model density to obtain an optimized neutron density for the Sn isotopes that can reproduce the experimental (p, p) data. Structural properties such as the surface neutron densities and the rms radii of the neutron densities in the Sn isotopes are also discussed, which suggest the shell effect at $N = 66$ in the Sn isotopes.

The paper is organized as follows. The structure and reaction calculations are explained in Sec. II, and the results obtained using the theoretical densities are presented in Sec. III. In Sec. IV, the isotopic analysis is performed using a model density to obtain the optimized density, and the results obtained are discussed. Finally, a summary is given in Sec. V.

II. CALCULATIONS OF NUCLEAR STRUCTURE AND PROTON ELASTIC SCATTERING

A. Structure calculations

Structure calculations for even-even Sn isotopes from ^{114}Sn to ^{124}Sn were performed by employing both RHB and SHFB calculations of spherical nuclei using the computational DIRHB code [24] and HFBRAD code [25], respectively. The spherical assumption is reasonable because most mean-field calculations obtain the ground states in this range of mass numbers with only weak or no deformation of the Sn isotopes. In the RHB calculations, the DD-ME2 [26] and DD-PC1 [27] interactions were used, which are simply denoted as me2 and pc1, respectively, in this paper. In the SHFB calculation, the SKM* [28] interaction with a mixed-type pairing force was used. The SHFB calculations with the SLy4 [29] interaction were also performed to check the interaction dependence, but the resulting densities of the Sn isotopes were similar to those obtained using the SKM* interaction; therefore, only the SKM* result are presented in this paper. Note that these structure models were tuned to fit the binding energies and rms charge radii globally over a wide range of mass numbers extending from ^{40}Ca to ^{208}Pb .

B. Calculations of proton elastic scattering reactions

$\text{Sn}(p, p)$ reactions at $E_p = 295$ MeV were calculated using the RIA+ddMH model, which is a modified version of the RIA+MH model proposed by Sakaguchi *et al.* [22]. In the RIA+MH and RIA+ddMH models, real and imaginary nucleon-nucleus potentials are constructed by

folding the target density with effective NN interactions of the meson-exchange model. The effective NN interaction in the original RIA+MH model contains energy dependences in the meson masses and coupling constants, and it was tuned to fit proton elastic scattering data globally over the energy range of $100 \text{ MeV} \leq E_p \leq 400 \text{ MeV}$. In the RIA+ddMH model, density-dependent σ - and ω -meson masses and coupling constants were introduced into the original effective NN interaction of the relativistic Love-Franey (RLF) parametrization [19, 20]. The density dependence is considered to be “a medium effect” of the effective NN interaction, which contains various many-body effects that occur in proton elastic scattering such as Pauli blocking, multistep processes, and the medium effects on meson properties. The parameterization of the density dependence of the RIA+ddMH model has been calibrated to fit the $^{58}\text{Ni}(p, p)$ data at 295 MeV, and it has been updated in Refs. [5, 7] from the original version [22]. In the present work, latest parameterization of the RIA+MH model determined in Ref. [7] was used, which afforded better reproduction of the $^{58}\text{Ni}(p, p)$ data in the range of $\theta_{\text{c.m.}} \lesssim 50^\circ$ than an earlier version [5] used for the analysis of $\text{Sn}(p, p)$ reactions.

The RIA+ddMH calculation was performed using the theoretical densities of Sn the isotopes. In an additional case, the RIA+MH calculations with the RLF parametrization and the Pauli-blocking effect were performed to check the model dependence in the reaction calculations. In the reaction calculations, the proton-nucleus potentials are obtained by folding the vector and scalar densities of the target nuclei with the effective NN interaction. The theoretical neutron ($\rho_n(r)$) and proton ($\rho_p(r)$) densities were used for the neutron and proton vector densities, whereas $0.96\rho_n(r)$ and $0.96\rho_p(r)$ of the theoretical densities were used for the neutron and proton scalar densities, respectively, consistently in the RHB and SHFB calculations. This treatment is the same as that done in the experimental analyses of Refs. [5, 7] and as adopted in my previous paper. Note that this prescription for the scalar density is considered a type of local-density approximation for the σ -meson exchange term of the effective NN interaction.

III. RESULTS

A. Densities and radii of Sn

The neutron (r_n) and proton (r_p) rms radii of the Sn isotopes using the RHB (me2 and pc1) and SHFB (SKM*) calculations are shown in Fig. 1 (a), together with the experimental data. In all calculations, r_p changes almost linearly as a function of the neutron number N along the isotope chain, and it reproduces the experimental data well. The theoretical values of r_n also exhibit a dependence of a linear function of N . In Fig. 1 (b), the neutron, proton, and matter (r_m) rms radii obtained

from the me2 calculations are compared with linear functions of N (or $A^{1/3}$). The theoretical values of r_n and r_p can be fitted approximately by the linear functions $r_n = 3.396 + 0.0191N$ and $r_p = 4.093 + 0.0069N$, respectively, whereas r_m is fitted roughly by $0.947A^{1/3}$ fm. However, the experimental r_n values obtained from the (p,p) reaction at 295 MeV do not show such a smooth N dependence.

The theoretical neutron (ρ_n) and proton (ρ_p) densities of ^{116}Sn and ^{122}Sn are shown in Fig. 2, together with the experimental data from Ref. [5], in which ρ_n was extracted from the (p,p) reaction at 295 MeV and ρ_p was obtained from the charge density distribution determined from electron elastic scattering. The three calculations using me2, pc1, and SKM* obtain ρ_p results approximately consistent with each other and that describe the experimental ρ_p results reasonably well. However, the theoretical ρ_n results depend somewhat on the calculations. As shown in Figs. 2 (c) and 2 (d), the position of the peak of $4\pi r^2 \rho_n(r)$ is shifted outward in the calculations that used the pc1 and SKM* densities compared with those utilizing the me2 density. These differences in the surface neutron densities in the region $4 \text{ fm} \lesssim r \lesssim 6 \text{ fm}$ produce differences among the theoretical predictions of the (p,p) cross sections at 295 MeV, as shown later, even though the me2, pc1, and SKM* calculations give approximately consistent values of r_n .

B. $\text{Sn}(p,p)$ cross sections at 295 MeV

Figure 3 shows the $\text{Sn}(p,p)$ cross sections at 295 MeV obtained from the RIA+ddMH calculations using the theoretical densities, together with the experimental data. The calculated cross sections at backward angles depend on the adopted theoretical density. Compared with the experimental cross sections, the me2 density yields reasonable agreement with the data, whereas the pc1 and SKM* densities do not; In the results for the pc1 and SKM* densities, the diffraction pattern has shrunk, because of the outward shift of the surface-peak position of $4\pi r^2 \rho(r)$ explained previously; hence, the positions of the dips at backward angles are shifted to forward angles and deviate significantly from the experimental data. This indicates that the (p,p) reactions at 295 MeV are good probes for determining the surface neutron density.

To see the dependence of the reaction calculations on the effective NN interaction model, the present RIA+ddMH and original RIA+MH calculations with the me2 density are compared in Fig. 4. Compared with RIA+MH, the RIA+ddMH calculations obtain a diffraction pattern that is expanded slightly toward larger angles, which means that the range of the NN interaction is effectively shorter in the RIA+ddMH model.

Among these theoretical calculations of the $\text{Sn}(p,p)$ reaction, the RIA+ddMH calculations with the me2 density obtains yield the best agreement with the experimental cross sections. In particular, they reproduce the

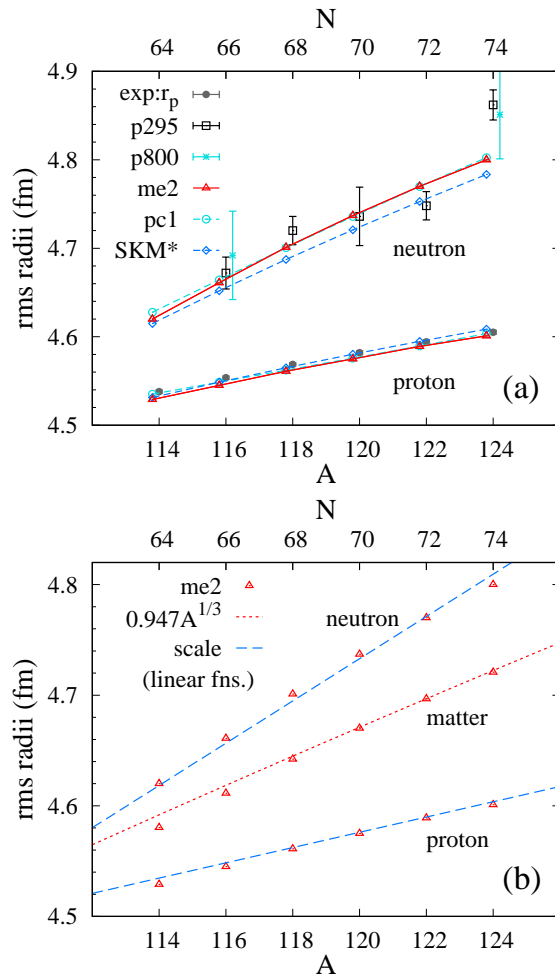


FIG. 1: (a) Rms radii of the neutron and proton density distributions in the Sn isotopes. The theoretical values are the RHB (me2 and pc1) calculations and the SHFB (SKM*) calculation. The experimental data are the r_n values obtained from the (p,p) reactions at both 295 MeV[5] and 800 MeV [4], and the r_p values are obtained from experimental data for the rms charge radii from isotope-shift measurements [30]. (b) The rms radii of the matter, proton, and neutron density distributions of the Sn isotopes obtained from the RHB (me2) calculations, together with the linear functions of $r_m = 0.947A^{1/3}$ fm, $r_n = 3.396 + 0.0191N$ fm, and $r_p = 4.093 + 0.0069N$ fm, which are adjusted to the theoretical values.

$^{122}\text{Sn}(p,p)$ cross sections fairly well. However, for the $^{116}\text{Sn}(p,p)$ and $^{118}\text{Sn}(p,p)$ cross sections, the agreement at backward angles is not satisfactory. This indicates that a modification of the theoretical densities of ^{116}Sn and ^{118}Sn from the me2 calculation is necessary to reproduce the (p,p) data.

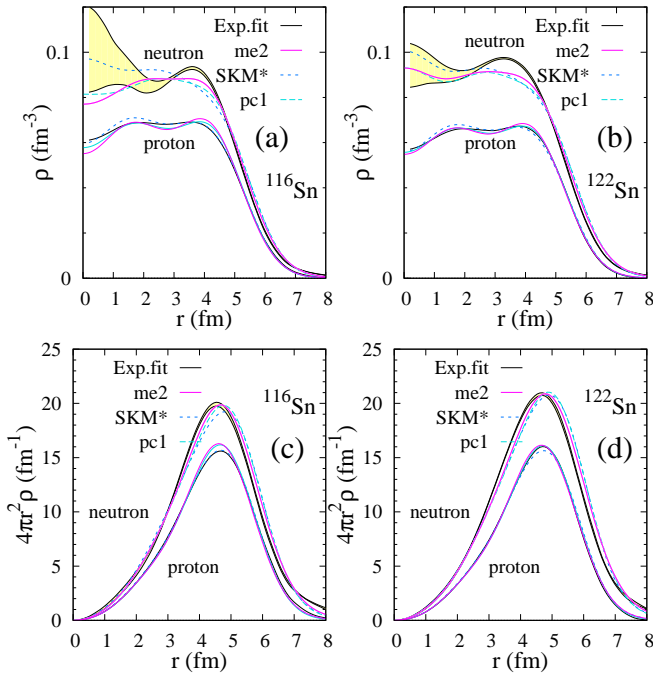


FIG. 2: Neutron (ρ_n^A) and proton (ρ_p^A) density distributions of ^{116}Sn and ^{122}Sn . Panels (a) and (b) show the neutron and proton density distributions for ^{116}Sn and ^{122}Sn , respectively, as obtained from the me2, pc1, and SKM* calculations, and panels (c) and (d) show the corresponding values of $4\pi r^2 \rho$. The experimental neutron and proton densities from Ref. [5] are also shown. The neutron density (error envelopes surrounded by thin lines) is extracted from proton elastic scattering at 295 MeV and the proton density (thin lines) is obtained from the charge distribution determined from electron elastic scattering.

C. Renormalization of the experimental cross sections

As discussed previously, the $\text{Sn}(p,p)$ cross sections at backward angles are sensitive to the surface neutron density of the target nucleus and also depend on the effective NN interaction used in the reaction calculations. However, the model dependence at forward angles is quite small; there is almost no difference between the calculations in the region $\theta_{c.m.} \lesssim 16^\circ$, as shown in Figs. 3 and 4. All the calculations reproduce the $^{116}\text{Sn}(p,p)$, $^{118}\text{Sn}(p,p)$, and $^{122}\text{Sn}(p,p)$ cross sections at forward angles reasonably well but cannot describe the $^{120}\text{Sn}(p,p)$ nor the $^{124}\text{Sn}(p,p)$ data. In the experimental data for the $^{120}\text{Sn}(p,p)$ and $^{124}\text{Sn}(p,p)$ cross sections, the peak height at $\theta_{c.m.} \approx 13^\circ$ is significantly smaller than expected from the isotopic systematic than are those for the other Sn isotopes.

To show this inconsistency in the data in more detail, the Rutherford ratios of the (p,p) cross sections are compared in linear plots for the five Sn isotopes in

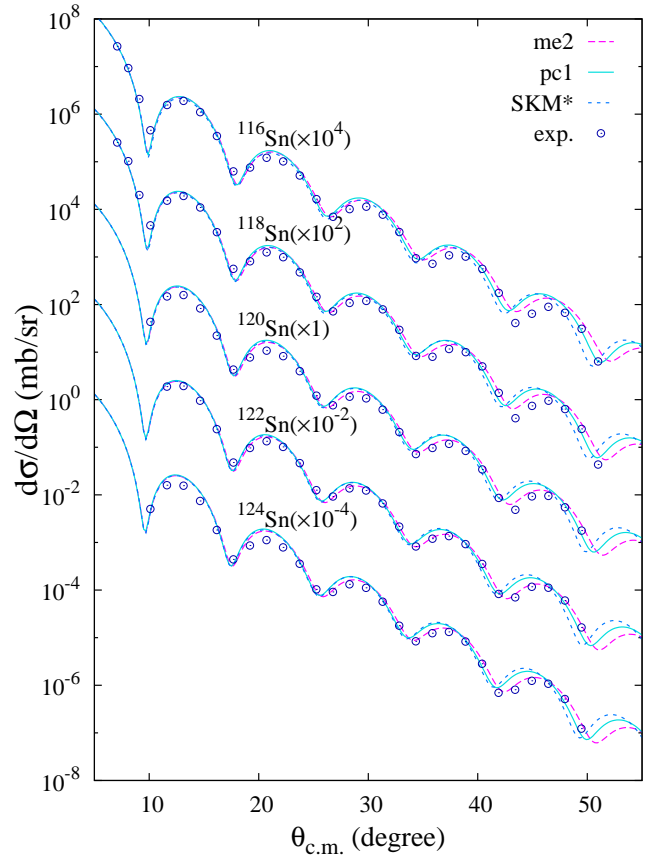


FIG. 3: $\text{Sn}(p,p)$ cross sections at 295 MeV obtained from the RIA+ddMH calculations using the theoretical densities from the me2, pc1, and SKM* calculations, together with the experimental data [5].

Figs. 5 (a) and 5 (b). The theoretical cross sections obtained from the RIA+ddMH calculation with the me2 density show reasonably systematic variations over the series of Sn isotopes; the peak position changes slightly but gradually to forward angles from ^{116}Sn to ^{124}Sn because of the increasing nuclear size, but the peak height is almost unchanged. However, in the experimental data, the peak heights of the $^{120}\text{Sn}(p,p)$ and $^{124}\text{Sn}(p,p)$ cross sections are about 20% smaller than those for the other Sn isotopes. Because the Rutherford ratio of the cross sections at the forward-angle peak usually close to unity for the (p,p) reactions, the experimental cross sections for $^{120}\text{Sn}(p,p)$ and $^{124}\text{Sn}(p,p)$ seem unexpectedly small, indicating that the normalization of these data should be corrected. Therefore, the $^{120}\text{Sn}(p,p)$ and $^{124}\text{Sn}(p,p)$ data were renormalized by multiplying them by factors of 1.20 and 1.27, respectively, to adjust the theoretical values $\sigma(^A\text{Sn})/\sigma(^{122}\text{Sn})$ of the cross section ratios for $^A\text{Sn}(p,p)$ to $^{122}\text{Sn}(p,p)$ at $\theta_{c.m.} = 13.14^\circ$ obtained from

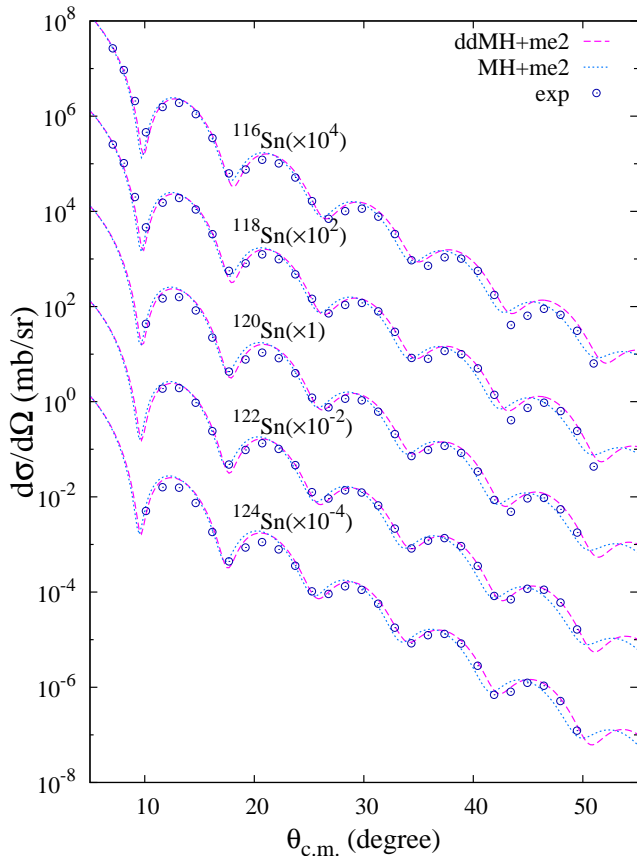


FIG. 4: $\text{Sn}(p,p)$ cross sections at 295 MeV obtained from the RIA+MH calculations using the me2 density compared with those obtained from the RIA+ddMH calculations and with the experimental data [5].

the RIA+ddMH calculations with the me2 density. As shown in Fig. 5 (c), the renormalized data for the cross sections show a reasonably systematic variation over the series of Sn isotopes. This calibration of the normalization of the $^{120}\text{Sn}(p,p)$ and $^{124}\text{Sn}(p,p)$ data using the theoretical prediction has almost no model dependence because all the calculations show quite similar isotopic systematics for the forward-angle cross sections; the model uncertainties in the normalization are less than a few percent. In the following analysis, the renormalized data are mainly used for the $^{120}\text{Sn}(p,p)$ and $^{124}\text{Sn}(p,p)$ cross sections.

D. Isotopic properties of nuclear structure and reactions

Here, the structural properties of the Sn isotopes in the region $A = 114$ – 124 obtained from the me2 calculations

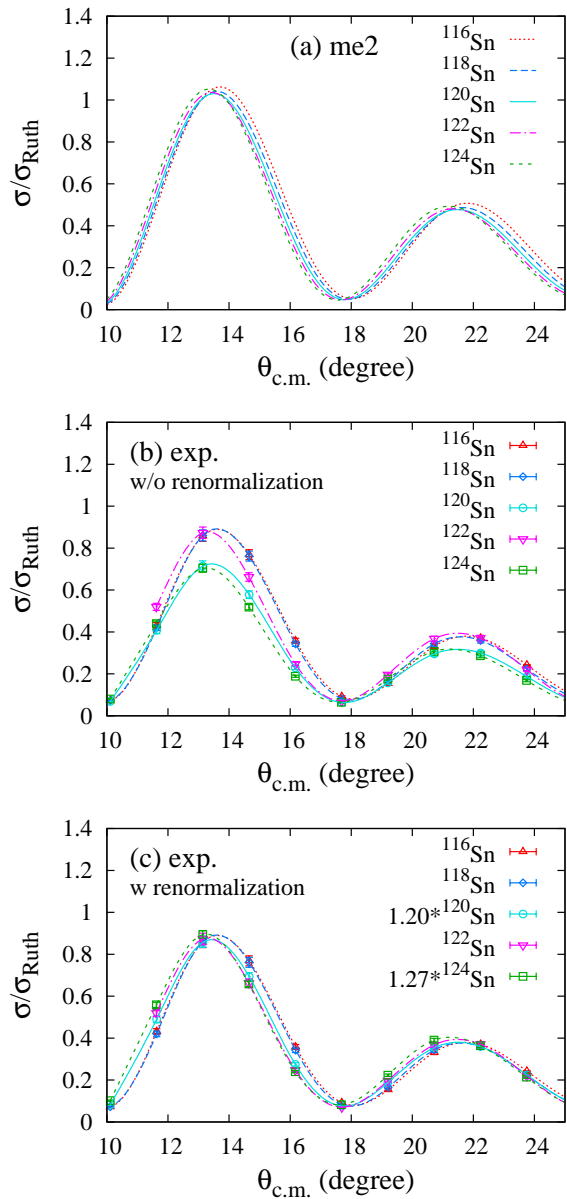


FIG. 5: (a) Rutherford ratios of the $\text{Sn}(p,p)$ cross sections at 295 MeV obtained from the RIA+ddMH calculations using the me2 density and (b) from the experimental data [5]. (c) The Rutherford ratio for the data from the original $^{120}\text{Sn}(p,p)$ and $^{124}\text{Sn}(p,p)$ cross sections of Ref. [5] renormalized by the factors 1.20 and 1.27, respectively. The experimental data points with error bars are connected by spline curves.

and their effects on the (p,p) cross sections are discussed while focusing on the isotopic systematics.

1. Structural properties

As discussed in Ref. [31], RHB calculations using such interactions as me2 and pc1 show features of neutron sub-

shell closure at ^{114}Sn because of the neutron-shell gap at $N = 64$, although the signal is not especially remarkable. In the range $A = 116\text{--}124$, from ^{116}Sn to ^{124}Sn , the valence neutrons occupy the $3s_{1/2}$, $2d_{3/2}$, and $1h_{11/2}$ orbits in the major shell on top of the ^{114}Sn core. These valence-neutron orbits contribute to the surface neutron density in the Sn isotopes. The theoretical results for the proton and neutron densities and valence-neutron densities obtained from the me2 calculations are shown in Fig. 6; Figures 6 (a) and 6 (b) shows $\rho_{n,p}(r)$ and $4\pi r^2 \rho_{n,p}(r)$, respectively, whereas Fig. 6 (c) shows the valence neutron density, $\rho_{\text{val}}(r) \equiv \rho_n^A(r) - \rho_n^{114}(r)$, and Fig. 6 (d) shows the valence neutron density per neutron, $\rho_{\text{val}}/N_{\text{val}}$ with $N_{\text{val}} = N - 64$. Here $\rho_{n(p)}^A(r)$ indicates the neutron (proton) density of ^ASn obtained from the me2 calculation. The single-particle densities of the major-shell orbits— $3s_{1/2}$, $2d_{3/2}$, and $1h_{11/2}$ —in ^{120}Sn are also shown in Fig. 6 (d). The surface neutron density changes gradually from ^{116}Sn to ^{124}Sn and the peak position of $4\pi r^2 \rho_n(r)$ shifts outward (in the large r direction) as valence neutrons increase, whereas the proton density is almost unchanged [Fig. 6 (a) and (b)]. The value of $4\pi r^2 \rho_{\text{val}}$ for the valence-neutron density shows an enhanced peak at $r \approx 6$ fm [Fig. 6 (c)]. In the valence-neutron density per neutron, $4\pi r^2 \rho_{\text{val}}/N_{\text{val}}$, there are small differences between isotopes in the region $r < 6$ fm, but there is almost no difference in the region $r \gtrsim 6$ fm [Fig. 6 (d)]. Such a weak N dependence of $\rho_{\text{val}}/N_{\text{val}}$ is consistent with the valence-neutron orbits in the major shell. Figure 7 shows the energies, occupation probabilities, and neutron numbers of single-particle orbits in the Sn isotopes. As shown in Figs. 7 (b) and 7 (c), the valence neutrons gradually occupy three major-shell orbits— $3s_{1/2}$, $2d_{3/2}$, and $1h_{11/2}$ —indicating that shell effects are smeared by the pairing effect. This isotopic systematic a surface neutron density that is smoothly changing from ^{116}Sn to ^{124}Sn can be described approximately by the radial scaling of a reference neutron density. To demonstrate this radial-scaling property, scaled densities $\rho_{n,\text{scale}}^A(r)$ and $\rho_{p,\text{scale}}^A(r)$ for the neutron and proton densities of ^ASn were constructed from $\rho_{n,p}^{122}(r)$ for the reference isotope ^{122}Sn ;

$$\rho_{n,\text{scale}}^A(r) = \frac{N}{72} \frac{1}{s_n^3} \rho_n^{122}(r/s_n), \quad (1)$$

$$\rho_{p,\text{scale}}^A(r) = \frac{1}{s_p^3} \rho_p^{122}(r/s_p), \quad (2)$$

where the radial scaling parameters s_n and s_p are chosen to be linear functions— $s_n = 1 + 0.004(N - 72)$ and $s_p = 1 + 0.0015(N - 72)$ —that fit the theoretical values of r_n and r_p , respectively, as shown in Fig. 1 (b). We label the scaled density as the me2-scale density. The valence-neutron density, $4\pi r^2 \rho_{\text{val}} = \rho_{n,\text{scale}}^A(r) - \rho_n^{114}(r)$ ($A = 116\text{--}124$), for the me2-scale density is shown in Fig. 6 (c), and the Sn(p, p) cross sections at 295 MeV obtained from the RIA+ddMH calculations using the me2-scale density are shown in Fig. 8 (a), for comparison with the results using the me2 density. The me2-scale density

describes the property of $4\pi r^2 \rho_{\text{val}}$ around the peak and yields (p, p) cross sections that are almost equivalent to those obtained using the me2 density. This indicates that the essential features of the surface neutron density obtained from the me2 calculations are simply described by radial scaling with a linear function.

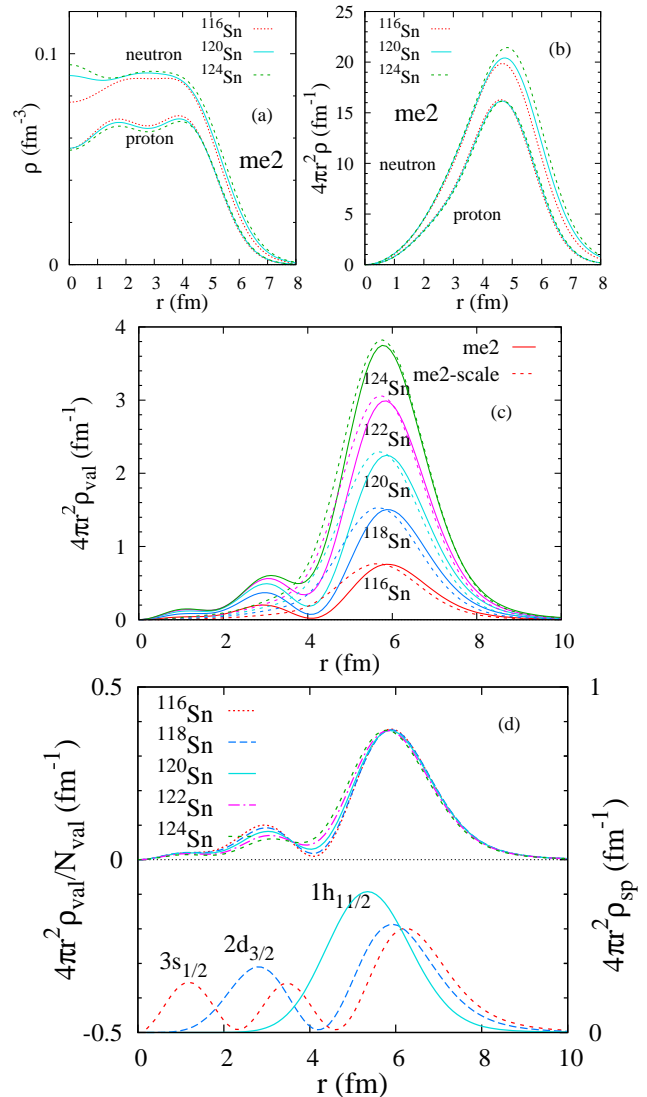


FIG. 6: (a) The neutron and proton density distributions of the Sn isotopes obtained from the me2 calculations and (b) the corresponding values of $4\pi r^2 \rho_{n,p}(r)$. (c) The valence neutron density $\rho_{\text{val}} \equiv \rho_n^A - \rho_n^{114}$ around the ^{114}Sn core for the me2 density. The density $\rho_{n,\text{scale}}^A(r) - \rho_n^{114}(r)$ for the me2-scale density is also shown for comparison. (d) (upper panel) The valence neutron density per neutron $\rho_{\text{val}}/N_{\text{val}}$ ($N_{\text{val}} = N - 64$) and (lower panel) the single-particle densities $\rho_{\sigma}^{s,p}(r)$ for $\sigma = 3s_{1/2}$, $2d_{3/2}$, and $1h_{11/2}$ in ^{120}Sn obtained from the me2 calculations.

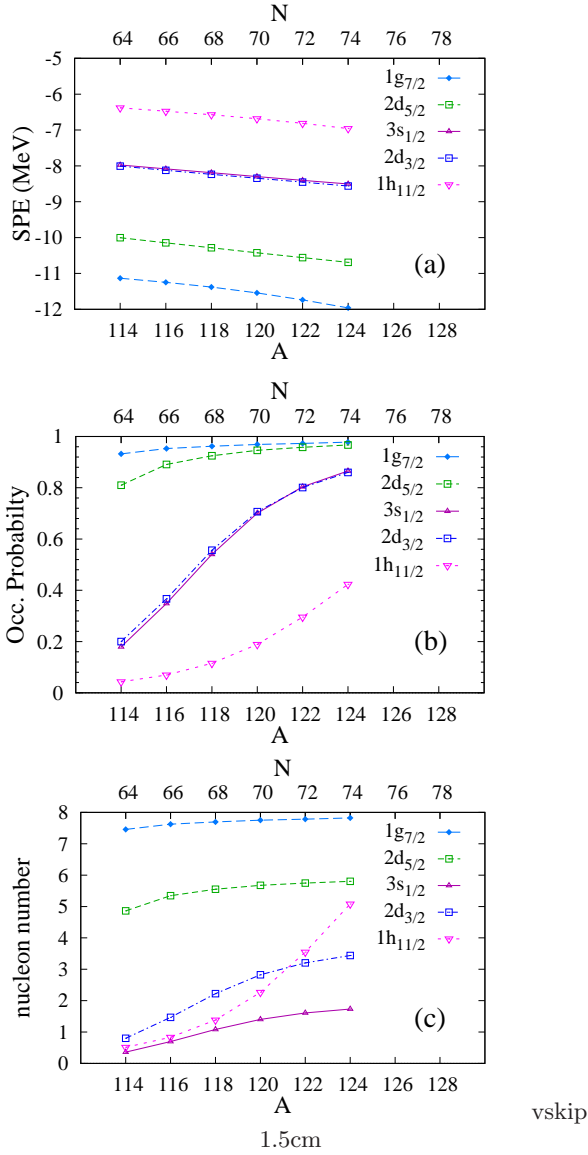


FIG. 7: (a) Neutron single-particle energies (SPE), (b) occupation probabilities, and (c) the number of neutrons in the single-particle orbits in the Sn isotopes obtained from the me2 calculations.

2. Sensitivity of (p,p) cross sections to the neutron structure

As explained previously, the RIA+ddMH calculations with the me2 density reproduce the experimental data for the $\text{Sn}(p,p)$ cross sections at 295 MeV reasonably well but overestimate the absolute amplitudes of the $^{116}\text{Sn}(p,p)$ and $^{118}\text{Sn}(p,p)$ cross sections at backward angles although they do describe the dip positions.

This indicates that some modification of the me2 density is needed for ^{116}Sn and ^{118}Sn . The essential feature that contributes to the cross sections is the surface neutron density, which is sensitive to the valence-neutron orbits in the major shell. To see the effects from each

major-shell orbit to the (p,p) cross sections at 295 MeV, modified neutron densities were constructed from the me2 density by replacing part of the neutron density in the original me2 density for ^ASn with a two-neutron density in the $3s_{1/2}$, $2d_{3/2}$, or $1h_{11/2}$ orbit;

$$\rho_n^A(r) = \left(1 - \frac{2}{N}\right)\rho_n^A(r) + 2\rho_\sigma^{\text{s.p.}}(r), \quad (3)$$

where $\rho_\sigma^{\text{s.p.}}(r)$, with $\sigma = \{3s_{1/2}, 2d_{3/2}, 1h_{11/2}\}$, are the single-particle densities obtained for ^{120}Sn , which are shown in the lower panel of Fig. 6 (d). The (p,p) cross sections obtained using this modified density for the $(3s_{1/2})^2$, $(2d_{3/2})^2$, and $(1h_{11/2})^2$ cases are shown in Fig. 8 (b). In the result calculated for the $(3s_{1/2})^2$ case, the cross sections at backward angles are suppressed, and improved results are obtained for the $^{116}\text{Sn}(p,p)$ and $^{118}\text{Sn}(p,p)$ cross sections compared with the original me2 results. However, in the results for the $(2d_{3/2})^2$ and $(1h_{11/2})^2$ cases, the cross sections are almost unchanged from the me2 result. This means that the cross sections are sensitive to $3s_{1/2}$ neutrons, as expected from the general trend of higher nodal orbits that provide significant contributions to the surface neutron density.

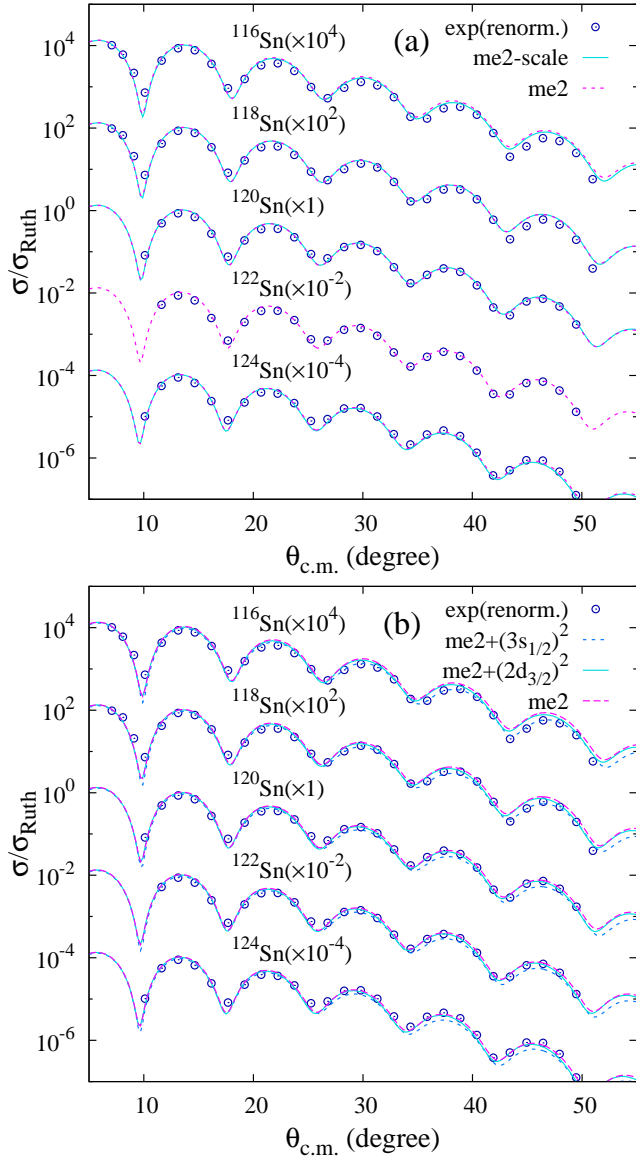


FIG. 8: (a) $\text{Sn}(p,p)$ cross sections at 295 MeV obtained from the RIA+ddMH calculations using the me2 and me2-scale densities. (b) The cross sections obtained using the modified densities for the $(3s_{1/2})^2$ and $(2d_{3/2})^2$ cases together with the results obtained using the original me2 density. The renormalized data for the experimental cross sections [5] are also shown; the $^{120}\text{Sn}(p,p)$ and $^{124}\text{Sn}(p,p)$ cross sections are renormalized from the original data of Ref. [5] by factors of 1.20 and 1.27, respectively.

IV. ISOTOPIC ANALYSIS OF CROSS SECTIONS USING MODEL DENSITY

To fine tune the neutron density to fit the (p, p) cross section data, I introduce a model density that extends the modified density with $(3s_{1/2})^2$ neutrons. This corresponds to a modification of the me2 density and is called the me2-3s model. In the me2-3s model, the neutron density $\rho_{n,3s}^A(r)$ is expressed as

$$\rho_{n,3s}^A(r) = \frac{1}{(1 + \delta_s)^3} \cdot \left\{ \left(1 - \frac{v}{N}\right) \rho_n^A \left(\frac{r}{1 + \delta_s}\right) + v \rho_{3s_{1/2}}^{s.p.} \left(\frac{r}{1 + \delta_s}\right) \right\} \quad (4)$$

with the two parameters v and δ_s that respectively indicate the enhancement of the $3s_{1/2}$ neutron density and the radial (r) scaling, respectively. The case $v = 2$ with $\delta_s = 0$ (no scaling) corresponds to the modified density for the $(3s_{1/2})^2$ case from the previous discussion. Note that the parameter v does not directly correspond to an increase in the density of $3s_{1/2}$ neutrons, but it effectively controls the contribution of the $3s_{1/2}$ neutrons to the neutron density. The isotopic analysis of $^A\text{Sn}(p, p)$ at 295 MeV was performed using the RIA+ddMH calculation with the me2-3s density.

For the isotopic analyses of the neutron density and (p, p) cross sections, the isotopic neutron density difference and the isotopic cross section ratio are defined by adopting ^{122}Sn as the reference isotope;

$$D(\rho_n; r) \equiv \rho_n(^A\text{Sn}; r) - \rho_n(^{122}\text{Sn}; r), \quad (5)$$

$$R(\sigma; \theta_{c.m.}) \equiv \frac{d\sigma(^A\text{Sn})/d\Omega}{d\sigma(^{122}\text{Sn})/d\Omega}, \quad (6)$$

where $d\sigma(^A\text{Sn})/d\Omega$ are the differential cross sections for the $^A\text{Sn}(p, p)$ reactions in the center-of-mass frame. The experimental values of $R(\sigma; \theta_{c.m.})$ are obtained from the $\text{Sn}(p, p)$ cross section data measured at the same angles in the laboratory frame omitting a slight difference in the angles in the center-of-mass frame caused by the mass difference between isotopes.

Figure 9 shows the isotopic cross section ratio $R(\sigma)$ for $^A\text{Sn}(p, p)$ at 295 MeV calculated using the me2 and me2-3s densities, together with the experimental values obtained from the (p, p) cross section data. Here, the result obtained using the me2 density, which is shown by the solid lines, is first discussed. The ratio $R(\sigma)$ shows an oscillating behavior that corresponds to a slight shift in the diffraction pattern of the cross sections from ^{122}Sn to ^ASn , which probes the change in nuclear size via the nucleon-nucleus optical potentials. As discussed in the previous analysis of Pb isotopes [23], the oscillation amplitude of $R(\sigma)$ is dominantly determined by the isotopic neutron-radius difference, whereas the gradual deviation from the line $R = 1$ is sensitive to the detailed profiles of the surface neutron density around the peak of $4\pi r^2 \rho_n(r)$. As N decreases from ^{122}Sn to ^{116}Sn , the

oscillation amplitude of $R(\sigma)$ increases because of the shrinking nuclear size. The opposite oscillation pattern of $R(\sigma)$ obtained for ^{124}Sn indicates that the nuclear size increases from ^{122}Sn to ^{124}Sn , but the oscillation amplitude is consistent with that for ^{120}Sn because the size difference from the reference isotope ^{122}Sn has almost the same magnitude for ^{120}Sn and ^{124}Sn .

Next, let me turn to the results obtained using the me2-3s model. In Fig. 9, the ratio $R(\sigma)$ obtained using the me2-3s density with $v = 2$ and $v = -1$ for the case $\delta_s = 0$ (no scaling) are shown by dashed and dotted lines, which respectively correspond to enhanced and suppressed $3s_{1/2}$ neutron components. In the result for ^{116}Sn , the me2-3s model with $(v, \delta_s) = (2, 0)$ yields a better agreement than the original me2 result, but a slight disagreement with the experimental data still remains. By tuning the radial scaling parameter δ_s , the me2-3s density with the parameter set $v = 2$ and $\delta_s = -0.7\%$ was obtained as an optimized solution to reproduce the experimental $R(\sigma)$ for ^{116}Sn . A similar analysis was performed for ^{118}Sn , and the optimized parameter set $(v, \delta_s) = (1.5, -0.7\%)$ was obtained to describe the experimental $R(\sigma)$.

For ^{120}Sn , the $R(\sigma)$ values obtained from the renormalized data for the $^{120}\text{Sn}(p, p)$ cross sections are successfully described by the calculations using the me2 density, indicating that no correction to the original me2 density is necessary. For ^{124}Sn , the $R(\sigma)$ values obtained from the renormalized data for the $^{124}\text{Sn}(p, p)$ cross sections can be described by the me2-3s density with $(v, \delta_s) = (-1, 0)$, which corresponds to a slight decrease in the $3s_{1/2}$ neutron density from the original me2 density. Note that the experimental $R(\sigma)$ obtained from the original $^{120}\text{Sn}(p, p)$ and $^{124}\text{Sn}(p, p)$ data without renormalization deviates significantly from $R = 1$, and it is difficult to be described it with these calculations.

To discuss the dependence of the present analysis of $R(\sigma)$ on the effective NN interaction model used in the reaction calculations, I perform the RIA+MH calculations using the me2 and me2-3s densities and compare the result with the RIA+ddMH calculations. As shown in Fig. 10 (a), the oscillation interval of $R(\sigma)$ is slightly shorter for the RIA+MH result than for RIA+ddMH. However, by rescaling the angles $\theta \rightarrow \theta^* = S_\theta \theta_{c.m.}$, almost consistent results are obtained for both calculations. Here the angle-scaling factor is chosen to be $S_\theta = \theta_{4\text{th}}/\theta_{4\text{th}}^{\text{MH}}$ so as to fit the angle ($\theta_{4\text{th}}^{\text{MH}}$) of the fourth peak of the $^{122}\text{Sn}(p, p)$ cross sections obtained from the MH calculations to that of the ddMH calculations ($\theta_{4\text{th}}$). The θ^* plot of $R(\sigma)$ obtained from the RIA+MH calculations is shown in Fig. 10 (b). The optimized me2-3s density with $v = 2$ and $\delta = 0.7\%$ yields good agreement with the experimental values of $R(\sigma)$ for ^{116}Sn , indicating that the optimized neutron density can be extracted with less model uncertainty by fitting the experimental values of $R(\sigma)$ in the θ^* plot.

A. Structure and reaction properties with the optimized me2-3s model density

I call the set of neutron densities obtained using the me2-3s model with the optimized parameters $(v, \delta_s) = (2, -0.7\%)$, $(1.5, -0.7\%)$, $(0, 0)$, $(0, 0)$, and $(-1, 0)$ for ^{116}Sn , ^{118}Sn , ^{120}Sn , ^{122}Sn , and ^{124}Sn , respectively, the “me2-3s(optm)” densities, which are obtained in the present analysis by fitting the experimental $R(\sigma)$. Note that, for ^{120}Sn and ^{122}Sn , the me2-3s(optm) density is consistent with the original me2 density that reproduces the cross section data without modification. In this section, I discuss the $\text{Sn}(p, p)$ cross sections and the neutron structure properties obtained using the me2-3s(optm) density.

1. Cross sections and analyzing powers

The cross sections and analyzing powers of $\text{Sn}(p, p)$ at 295 MeV calculated with RIA+ddMH using the me2-3s(opt) density are shown in Figs. 11 and 12, respectively, in comparison with the experimental data and with the theoretical result obtained using the me2 density. The present me2-3s(optm) density successfully describes the experimental (p, p) data for the series of Sn isotopes from ^{116}Sn to ^{124}Sn . In particular, the reproduction of the $^{116}\text{Sn}(p, p)$ and $^{118}\text{Sn}(p, p)$ cross sections at backward angles is substantially improved by the modification from the me2 density to the me2-3s(optm) density.

2. Neutron rms radii and skin thickness

The neutron rms radii r_n and skin thicknesses Δr_{np} of the Sn isotopes obtained for the me2-3s(optm) density are shown in Fig. 13, together with other theoretical predictions and experimental values. The me2-3s(optm) density gives r_n and Δr_{np} values that are almost consistent with those of the me2 calculation, meaning that the modification of the surface neutron density from the me2 to me2-3s(optm) densities does not make an essential contribution to the neutron rms radii, although it affects the (p, p) reactions. The obtained values show smooth N dependences for r_n and Δr_{np} . This smooth increase in Δr_{np} with N increasing is consistent with an theoretical work for the microscopic description of the $\text{Sn}(p, p)$ reactions at 295 MeV[32], but seems to somewhat contradict the experimental N dependences of Ref. [5].

3. Neutron density and shell structure

Next, the detailed properties of the neutron densities of the Sn isotopes obtained using the me2-3s(optm) density are discussed. Figure 14 compares the values of $\rho_n^{116}(r)$ for the me2-3s(opt) density with $\rho_n^{116}(r)$ and $\rho_n^{122}(r)$ for the me2 density. Figures 14 (a) and 14 (c), respectively,

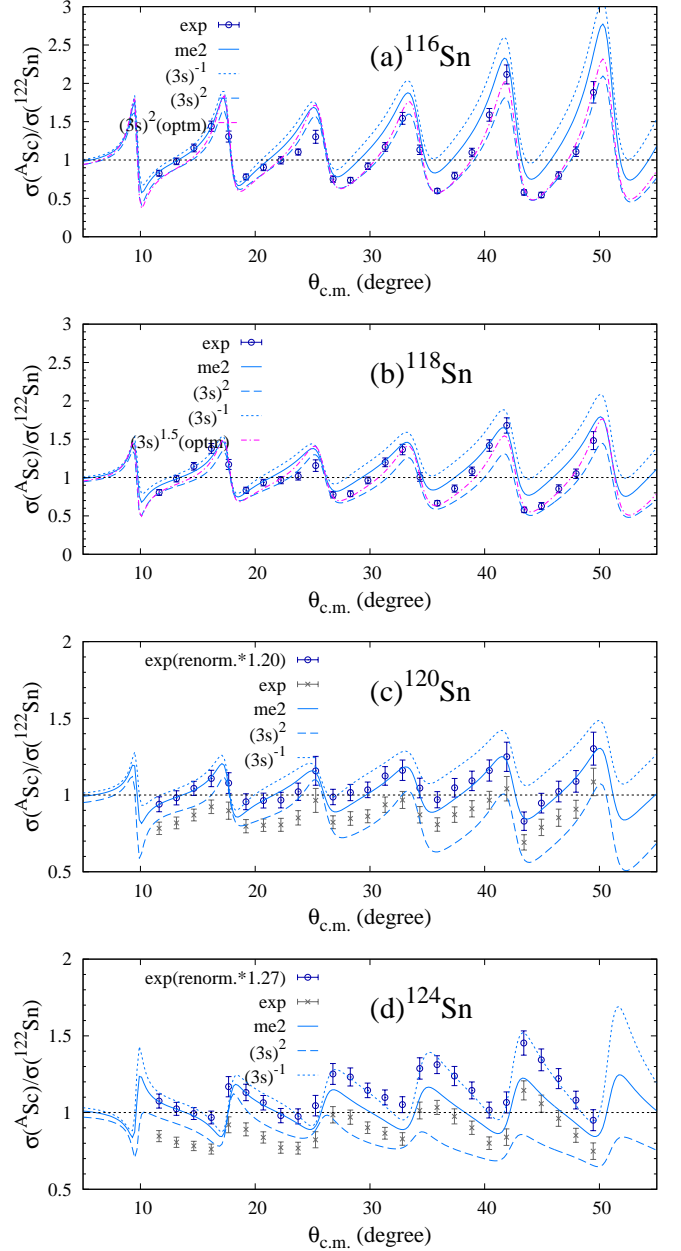


FIG. 9: Isotopic cross section ratio $R(\sigma)$ for $^A\text{Sn}(p, p)$ to $^{122}\text{Sn}(p, p)$ at 295 MeV obtained from the RIA+ddMH calculations using the me2-3s density with $(v, \delta_s) = (2, 0)$ and $(-1, 0)$ [labeled $(3s)^2$ and $(3s)^{-1}$, respectively]. In panels (a) and (b) for $^{116}\text{Sn}(p, p)$ and $^{118}\text{Sn}(p, p)$, the results obtained using the me2-3s density with the optimized parameter sets $(v, \delta_s) = (2, -0.7\%)$ and $(v, \delta_s) = (1.5, -0.7\%)$ are also shown, with the labels $(3s)^2(\text{optm})$ and $(3s)^{1.5}(\text{optm})$, respectively. The experimental values of $R(\sigma)$ include those obtained using the original data of Ref. [5] and those obtained using the data for the $^{120}\text{Sn}(p, p)$ and $^{120}\text{Sn}(p, p)$ cross sections renormalized by the factors 1.20 and 1.27, respectively.

plot the quantities $\rho_n(r)$ and $4\pi r^2 \rho_n(r)$. To demonstrate the difference between the me2 and me2-3s(opt) den-

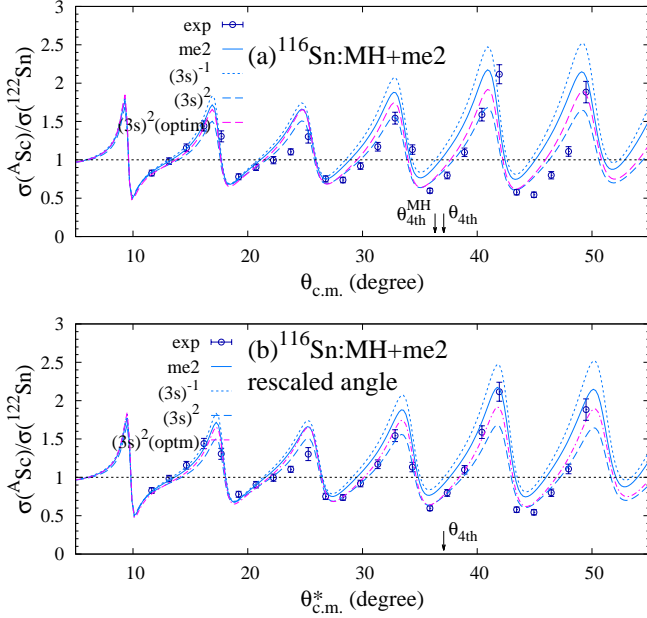


FIG. 10: (a) Same as Fig. 9(a) but using the results obtained from the RIA+MH calculations together with the experimental values. (b) The same ratios plotted against the rescaled angles $\theta_{c.m.}^* = S_\theta \theta_{c.m.}$ obtained with the angle-scaling factor $S_\theta = \theta_{4th} / \theta_{4th}^{MH}$. The angle θ_{4th} (θ_{4th}^{MH}) of the fourth peak of the $^{122}\text{Sn}(p,p)$ cross sections obtained from the RIA+ddMH (RIA+MH) calculations using the me2 density is shown by the arrows. The experimental values obtained from the cross section data of Ref. [5] are plotted for $\theta_{c.m.}$.

sities more clearly, the densities $\rho_n^{122}(r) - 3D(\rho_n)$ and $4\pi r^2(\rho_n^{122}(r) - 3D(\rho_n))$ are shown in Figs. 14 (b) and 14 (d), respectively, which correspond to three times enhancement of the isotopic neutron-density difference $D(\rho_n)$ of ^{116}Sn from ^{122}Sn . As shown in Figs. 14 (c) and 14 (d), the peak position of $4\pi r^2 \rho_n^{116}(r)$ obtained using the me2 density is shifted inward compared with that of $4\pi r^2 \rho_n^{122}(r)$. This change in the surface neutron density from ^{116}Sn to ^{122}Sn is described by the radial scaling $r \rightarrow r/s_n$ discussed previously. In the plot of $4\pi r^2 \rho_n^{116}(r)$ for the me2-3s(optm) density, the surface-peak amplitude in the region $4 \text{ fm} \lesssim r \lesssim 6 \text{ fm}$ is reduced from that obtained with the me2 density, whereas the peak position is almost unchanged. This reduction of the neutron density around the surface peak decreases the backward cross sections and improves the agreement with the experimental $^{116}\text{Sn}(p,p)$ data.

In Fig. 15, the isotopic neutron-density differences $D(\rho_n)$ of ^ASn from ^{122}Sn in the me2 and me2-3s(optm) densities are shown by dashed and solid lines, respectively. The correction of the surface neutron density from me2 to me2-3s(optm) can be clearly seen in the comparisons of $D(\rho_n)$. As shown in Figs. 15 (a) and 15 (b) for ^{116}Sn and ^{118}Sn , the amplitude of $4\pi r^2 D(\rho_n)$ in the region $4 \text{ fm} \lesssim r \lesssim 6 \text{ fm}$ increases, and the shape of the peak changes, in going from the original me2 to the me2-

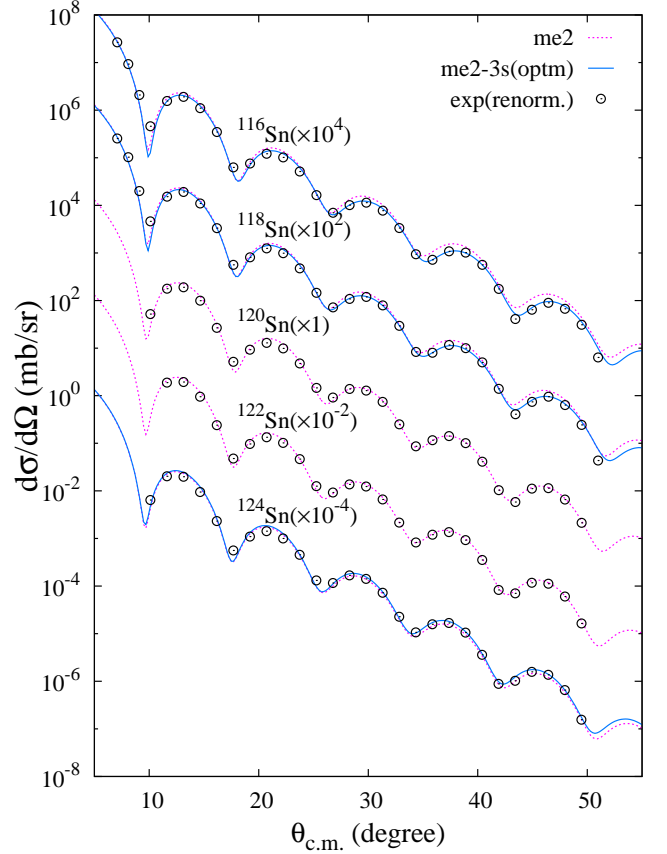


FIG. 11: Cross sections of $\text{Sn}(p,p)$ reactions at 295 MeV obtained from the RIA+ddMH calculations using the me2 and me2-3s(optm) densities together with the experimental data. The experimental data for the $^{120}\text{Sn}(p,p)$ and $^{124}\text{Sn}(p,p)$ cross sections are renormalized from the original data of Ref. [5] by factors of 1.20 and 1.27, respectively.

3s(optm) densities. This correction is essential for fitting the backward cross sections for the $^{116}\text{Sn}(p,p)$ reaction because $R(\sigma)$ is sensitive to $4\pi r^2 D(\rho_n)$ around the peak. The modification of the surface neutron density in the region $4 \text{ fm} \lesssim r \lesssim 6 \text{ fm}$ is described by the increase in the $3s_{1/2}$ neutron component, as is easily understood from the nodal structure of the $3s_{1/2}$ orbit. Indeed, in the simple case of the me2-3s model with $\delta_s = 0$, the change of $\rho_n(r)$ from the me2 density to the me2-3s density can be written as

$$\begin{aligned} \rho_{n,3s}(r) - \rho_n(r) &= D(\rho_{n,3s}) - D(\rho_n) \\ &= v(\rho_{3s_{1/2}}^{s.p.}(r) - \rho_n^A(r)/N). \end{aligned} \quad (7)$$

By thus combining the isotopic analyses of nuclear structure and reaction, it is concluded that the suppression of the $^{116}\text{Sn}(p,p)$ and $^{118}\text{Sn}(p,p)$ cross sections at backward

angles is the signal of an enhanced $3s_{1/2}$ neutron component, which is probed via its contribution to the surface neutron density and indicates the shell effect at $N = 66$ in the Sn isotopes.

TABLE I: Lowest configurations in the major shell, with the level ordering $\{3s_{1/2}, 2d_{3/2}, 1h_{11/2}\}$, for ^{116}Sn , ^{118}Sn , ^{120}Sn , ^{122}Sn , and ^{124}Sn and the corresponding hole configurations for the reference isotope ^{122}Sn .

Isotopes	Lowest config.	Hole config.
^{116}Sn	$(3s_{1/2})^2$	$(2d_{3/2})^{-4}(1h_{11/2})^{-2}$
^{118}Sn	$(3s_{1/2})^2(2d_{3/2})^2$	$(2d_{3/2})^{-2}(1h_{11/2})^{-2}$
^{120}Sn	$(3s_{1/2})^2(2d_{3/2})^4$	$(1h_{11/2})^{-2}$
^{122}Sn	$(3s_{1/2})^2(2d_{3/2})^4(1h_{11/2})^2$	reference
^{124}Sn	$(3s_{1/2})^2(2d_{3/2})^4(1h_{11/2})^4$	$(1h_{11/2})^2$

To discuss the shell effect, I consider the lowest configurations in the major shell, with the level ordering $\{3s_{1/2}, 2d_{3/2}, 1h_{11/2}\}$, without pairing. The lowest configurations for ^{116}Sn , ^{118}Sn , ^{120}Sn , ^{122}Sn , and ^{124}Sn are listed in Table I, together with the corresponding hole configurations for the reference ^{122}Sn state. In Fig. 15, the values of $4\pi r^2 D(\rho_n)$ for the lowest configurations are shown by dotted lines, which are perturbatively calculated using $\rho_{\sigma}^{\text{s.p.}}(r)$ in ^{120}Sn . As shown in Figs. 15 (a) and 15 (b), the lowest configurations of $(3s_{1/2})^2$ and $(3s_{1/2})^2(2d_{3/2})^2$ for ^{116}Sn and ^{118}Sn , respectively, can describe the peak shape of $4\pi r^2 D(\rho_n)$ obtained for the me2-3s(optm) density, although they slightly underestimate the overall factor by about 20%. This result again supports the shell effect at $N = 66$ in the Sn isotopes. Strictly speaking, however, the present result cannot exclude the possibility of a vanishing shell gap at $N = 64$ between the $3s_{1/2}$ and $(1g_{7/2}, 2d_{5/2})$ orbits. To confirm this, experimental data that include the $^{114}\text{Sn}(p,p)$ reaction are needed.

For ^{120}Sn , the lowest configuration fails to describe the structure of $4\pi r^2 D(\rho_n)$ with the me2 density. Alternatively, the hole configuration $(2d_{3/2})^{-1}(1h_{3/2})^{-1}$ can describe the feature of $4\pi r^2 D(\rho_n)$, which means that configuration mixing between $2d_{3/2}$ and $1h_{11/2}$ may exist at $N \sim 70$. In the present me2-3s model, discussing details of the occupation probability for each orbit is difficult because higher-order effects from other orbits are effectively renormalized in the two parameters v and δ_s . Moreover, the (p,p) reaction at 295 MeV is insensitive to the $1d_{3/2}$ and $1h_{11/2}$ neutron components as discussed previously.

V. SUMMARY

Proton elastic scattering at 295 MeV off Sn isotopes in the range $A = 116$ – 124 was investigated using the

RIA+ddMH model with theoretical densities for the Sn isotopes obtained from both RHB and SHFB calculations of spherical nuclei. The isotopic systematics of the nuclear structure and the reaction cross sections were investigated for the series of Sn isotopes. The theoretical results from the structure calculations show a smooth A dependence of the neutron rms radii and surface densities, along the isotope chain because of the pairing effect. The RIA+ddMH calculations using the theoretical density from the RHB calculations with the me2 interaction (the so called DD-ME2 interaction) reasonably agreed with the experimental cross sections and analyzing powers—in particular, for the $^{122}\text{Sn}(p,p)$ reaction—but they overestimated the backward cross sections of the $^{116}\text{Sn}(p,p)$ and $^{118}\text{Sn}(p,p)$ reactions.

To obtain the optimized neutron density from the experimental Sn(p,p) data at 295 MeV, an isotopic analysis was performed based on the RIA+ddMH calculations using the me2-3s model, in which the original me2 density was modified by changing the $3s_{1/2}$ neutron component. The increase in the $3s_{1/2}$ neutron component made a significant contribution to the surface neutron density and improved the agreement with the experimental data for the $^{116}\text{Sn}(p,p)$ and $^{118}\text{Sn}(p,p)$ cross sections at backward angles. In other words, the suppression of the backward cross sections of the $^{116}\text{Sn}(p,p)$ and $^{118}\text{Sn}(p,p)$ reactions is the signal of an enhanced $3s_{1/2}$ neutron component, indicating the shell effect at $N = 66$ in the Sn isotopes. The neutron rms radii and skin thicknesses obtained in the present analysis show a smooth N dependence along the isotope chain, and they are approximately consistent with the theoretical predictions of the RHB calculation with the me2 interaction. This seems to contradict the experimental results of Ref. [5].

In the experimental Sn(p,p) data at 295 MeV in Ref. [5], the normalization of the $^{120}\text{Sn}(p,p)$ and $^{124}\text{Sn}(p,p)$ cross section data was found to be inconsistent with the data for other isotopes, suggesting that they should be corrected. To extract further accurate values of the neutron skin thickness from the Sn(p,p) data, a reanalysis taking into account the isotopic systematics of the data observed at 295 MeV is needed.

Acknowledgments

This work was supported by Grants-in-Aid of the Japan Society for the Promotion of Science (Grant Nos. JP18K03617 and 18H05407) and by a grant of the joint research project of the Research Center for Nuclear Physics at Osaka University.

-
- [1] X. Roca-Maza, M. Centelles, X. Vinas, and M. Warda, *Phys. Rev. Lett.* **106**, 252501 (2011), arXiv:1103.1762 [nucl-th] .
- [2] X. Roca-Maza and N. Paar, *Prog. Part. Nucl. Phys.* **101**, 96 (2018), arXiv:1804.06256 [nucl-th] .
- [3] M. B. Tsang et al., *Phys. Rev. C* **86**, 015803 (2012), arXiv:1204.0466 [nucl-ex] .
- [4] L. Ray, *Phys. Rev. C* **19**, 1855 (1979), [Erratum: *Phys.Rev.C* **20**, 1212–1212 (1979)].
- [5] S. Terashima et al., *Phys. Rev. C* **77**, 024317 (2008).
- [6] V. E. Starodubsky and N. M. Hintz, *Phys. Rev. C* **49**, 2118 (1994).
- [7] J. Zenihiro et al., *Phys. Rev. C* **82**, 044611 (2010).
- [8] A. Trzcinska, J. Jastrzebski, P. Lubinski, F. J. Hartmann, R. Schmidt, T. von Egidy, and B. Klos, *Phys. Rev. Lett.* **87**, 082501 (2001).
- [9] B. Klos et al., *Phys. Rev. C* **76**, 014311 (2007), arXiv:nucl-ex/0702016 .
- [10] S. Abrahamyan et al., *Phys. Rev. Lett.* **108**, 112502 (2012), arXiv:1201.2568 [nucl-ex] .
- [11] E. Friedman, *Nucl. Phys. A* **896**, 46 (2012), arXiv:1209.6168 [nucl-ex] .
- [12] C. M. Tarbert et al., *Phys. Rev. Lett.* **112**, 242502 (2014), arXiv:1311.0168 [nucl-ex] .
- [13] A. Krasznahorkay et al., *Phys. Rev. Lett.* **82**, 3216 (1999).
- [14] A. Tamii et al., *Phys. Rev. Lett.* **107**, 062502 (2011), arXiv:1104.5431 [nucl-ex] .
- [15] J. Piekarewicz, B. K. Agrawal, G. Colo, W. Nazarewicz, N. Paar, P. G. Reinhard, X. Roca-Maza, and D. Vretenar, *Phys. Rev. C* **85**, 041302 (2012), arXiv:1201.3807 [nucl-th] .
- [16] L. Ray, W. R. Coker, and G. W. Hoffmann, *Phys. Rev. C* **18**, 2641 (1978).
- [17] G. W. Hoffmann et al., *Phys. Rev. C* **21**, 1488 (1980).
- [18] J. Zenihiro et al., (2018), arXiv:1810.11796 [nucl-ex] .
- [19] C. J. Horowitz, *Phys. Rev. C* **31**, 1340 (1985).
- [20] D. P. Murdock and C. J. Horowitz, *Phys. Rev. C* **35**, 1442 (1987).
- [21] C. Horowitz, D. Murdock, and S. B.D., *Computational Nuclear Physics 1*, edited by K. Langanke, J. Maruhn, and S. Koonin (Springer-Verlag, 1991) p. 129.
- [22] H. Sakaguchi et al., *Phys. Rev. C* **57**, 1749 (1998).
- [23] Y. Kanada-En'yo, (2021), arXiv:2106.00151 [nucl-th] .
- [24] T. Nikšić, N. Paar, D. Vretenar, and P. Ring, *Comput. Phys. Commun.* **185**, 1808 (2014), arXiv:1403.4039 [nucl-th] .
- [25] K. Bennaceur and J. Dobaczewski, *Comput. Phys. Commun.* **168**, 96 (2005), arXiv:nucl-th/0501002 .
- [26] G. A. Lalazissis, T. Nikšić, D. Vretenar, and P. Ring, *Phys. Rev. C* **71**, 024312 (2005).
- [27] T. Nikšić, D. Vretenar, and P. Ring, *Phys. Rev. C* **78**, 034318 (2008), arXiv:0809.1375 [nucl-th] .
- [28] J. Bartel, P. Quentin, M. Brack, C. Guet, and H. B. Hakansson, *Nucl. Phys. A* **386**, 79 (1982).
- [29] E. Chabanat, P. Bonche, P. Haensel, J. Meyer, and R. Schaeffer, *Nucl. Phys. A* **635**, 231 (1998), [Erratum: *Nucl.Phys.A* **643**, 441–441 (1998)].
- [30] I. Angeli and K. P. Marinova, *Atom. Data Nucl. Data Tabl.* **99**, 69 (2013).
- [31] Y. El Basseem and M. Oulne, *Nucl. Phys. A* **987**, 16 (2019), arXiv:1904.10318 [nucl-th] .
- [32] W. Haider, M. Sharma, Y. K. Gambhir, and S. Kailas, *Phys. Rev. C* **81**, 034601 (2010).

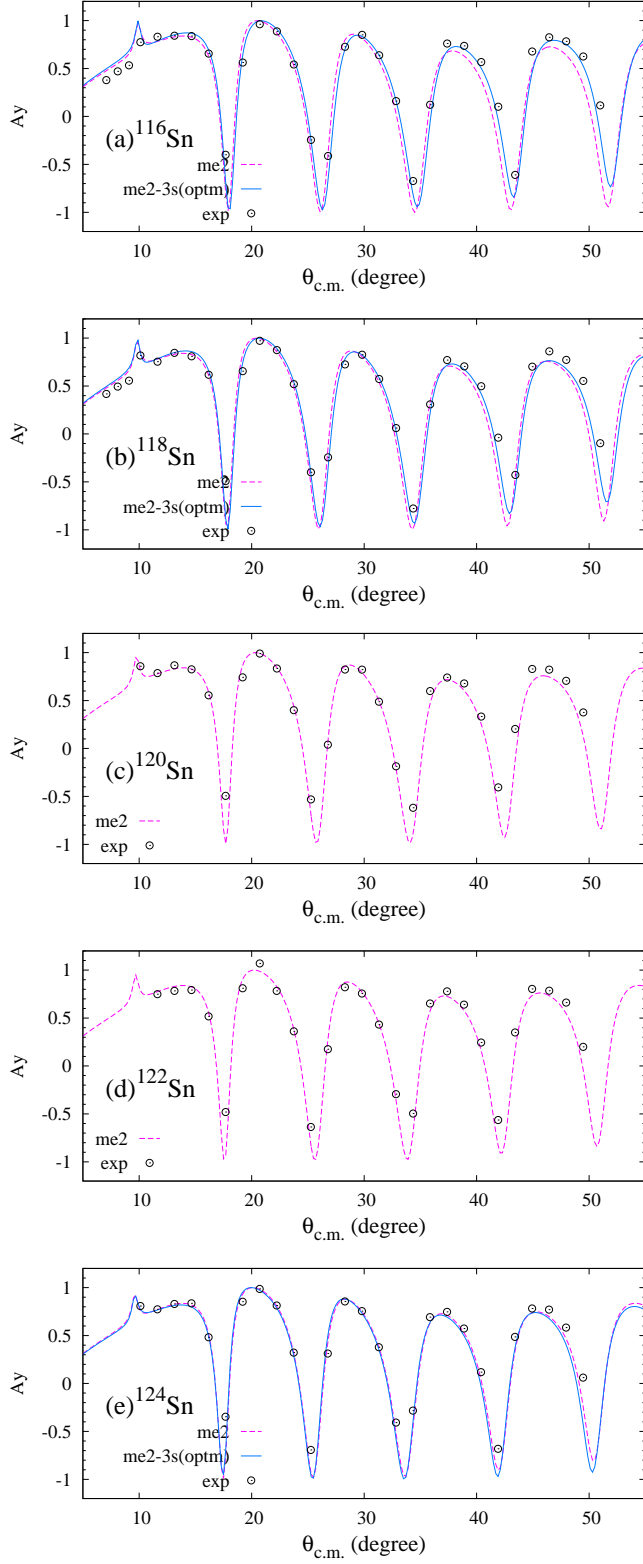


FIG. 12: Analyzing powers of $\text{Sn}(p,p)$ at 295 MeV obtained from the RIA+ddMH calculations using the me2 and me2-3s(optm) densities together with the experimental data [5].

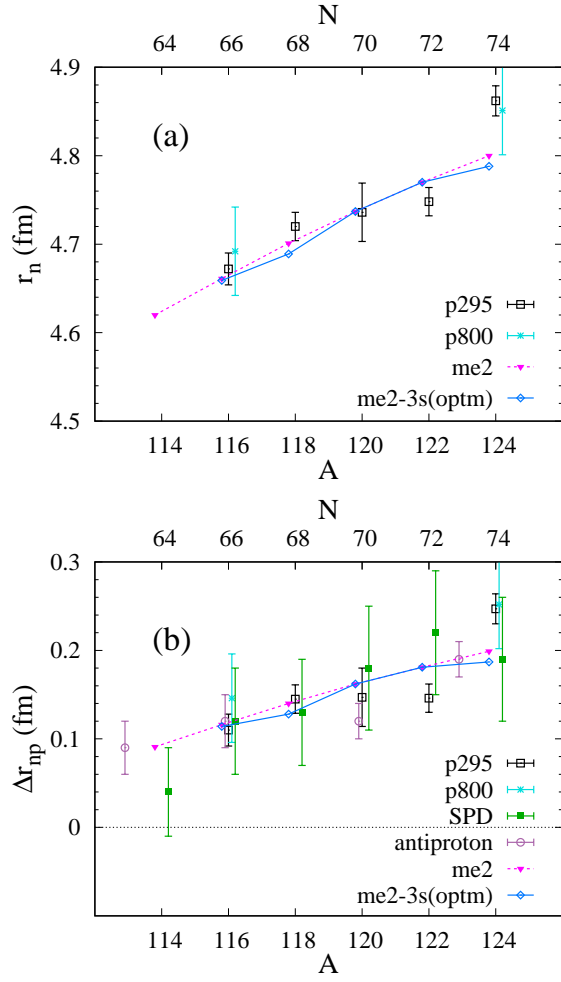


FIG. 13: (a) Neutron rms radii and (b) skin thicknesses of the Sn isotopes obtained from the me2 calculations and those obtained using the me2-3s(optm) density, together with the experimental data. The experimental data include the values of r_n and Δr_{np} obtained from the (p,p) reactions at both 295 MeV [5] and 800 MeV [4], as well as the Δr_{np} values obtained from x -ray data from antiprotonic atoms [8] and from spin-dipole resonances (SPD) measured using the $(^3\text{He}, t)$ charge-exchange reaction at 450 MeV [13].

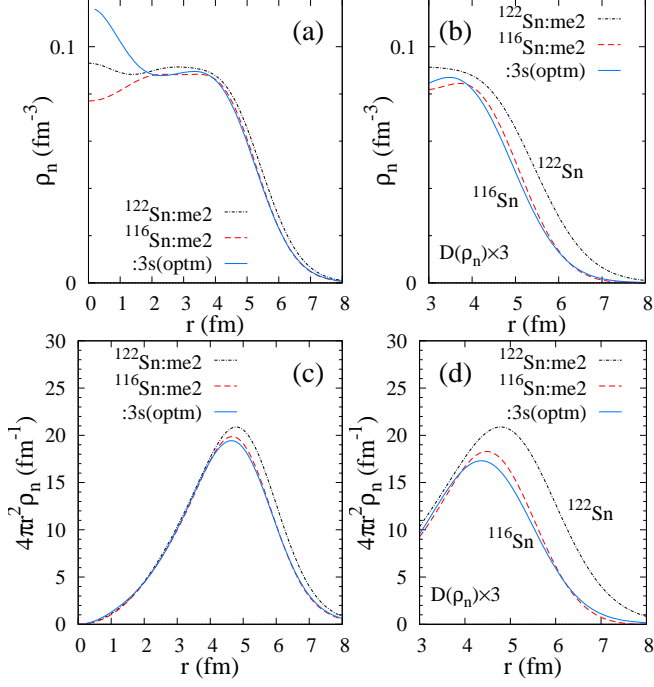


FIG. 14: (a) Neutron density distributions of ^{116}Sn obtained using the me2 and me2-3s(optm) model densities compared with the ^{122}Sn density. (b) The density $\rho_n^{122}(r) - 3D(\rho_n)$ corresponds to three times enhancement of the isotopic neutron difference $D(\rho_n)$ of ^{116}Sn from ^{122}Sn . Panels (c) and (d) show the corresponding values of $4\pi r^2 \rho_n(r)$ for (a) and (b), respectively, but $4\pi r^2 \rho_n(r)$.

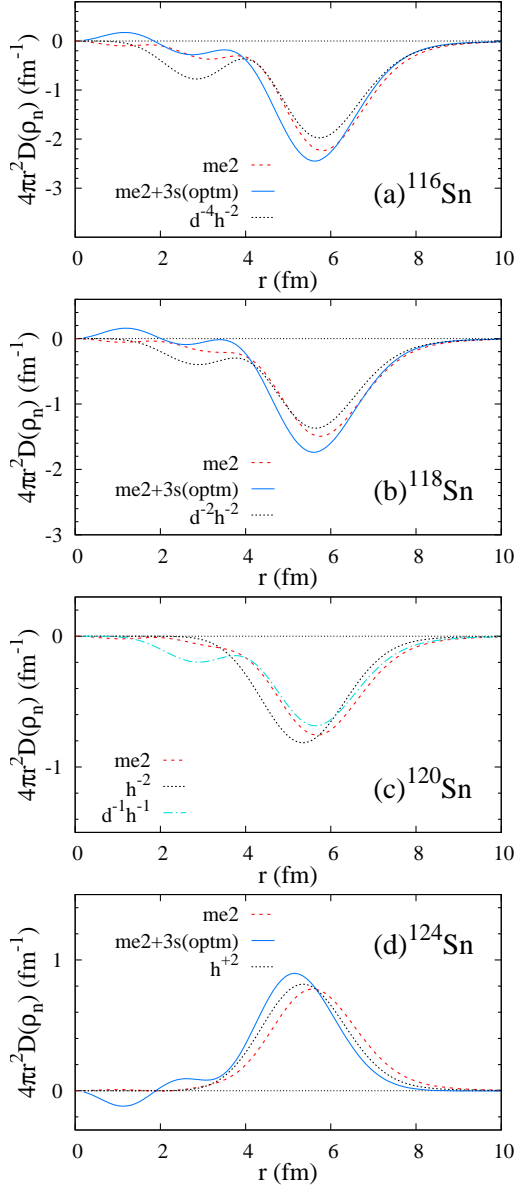


FIG. 15: Isotopic neutron-density difference of ${}^A\text{Sn}$ from ${}^{122}\text{Sn}$ obtained for the me2 and me2-3s(optm) densities. Those for the lowest configurations are also shown. The configurations are listed in Table I. Panel (c) also shows the hole density for the $(2d_{3/2})^{-1}(1h_{11/2})^{-1}$ configuration.